



Insights in the mechanism of selective olefin oligomerisation catalysis using stopped-flow freeze-quench techniques: A Mo K-edge QEXAFS study

Stuart A. Bartlett^a, Peter P. Wells^a, Maarten Nachtegaal^b, Andrew J. Dent^c, Giannantonio Cibin^c, Gillian Reid^a, John Evans^a, Moniek Tromp^{d,*}

^aSchool of Chemistry, University of Southampton, Highfield, Southampton SO17 1BJ, United Kingdom

^bPaul Scherrer Institut, 5232 Villigen, Switzerland

^cDiamond Light Source Ltd., Didcot OX11 0DE, United Kingdom

^dStrukturanalytik in der Katalyse, Chemie, Catalysis Research Center, Technische Universität München, Lichtenbergstrasse 4, 85748 Garching, Germany

ARTICLE INFO

Article history:

Available online 13 November 2011

Keywords:

Oligomerisation
Catalysis
XAS
Mechanism
Mo
Stopped-flow
Freeze-quench
Homogeneous

ABSTRACT

The activation of $[\text{MoX}_3(\text{L})]$ (with $\text{X} = \text{Cl}, \text{Br}$; $\text{L} =$ tridentate ligands with S_3 and SNS donor sets) by AlMe_3 , analogous to the industrially important $[\text{CrCl}_3(\text{L})]$ catalysts for selective oligomerisation of alkenes, has been investigated by Mo K-edge X-ray absorption (XAS) and UV–visible spectroscopies. Time-resolved stopped-flow XAS, in combination with a newly developed anaerobic freeze-quench approach, have established the complete alkylation of the Mo centres and a slower, stepwise sequence for $[\text{MoBr}_3(\text{L})]$. No evidence for directly bonded or bridged Mo–Mo dimers was observed at the high Mo: AlMe_3 ratios used in this study. Decomposition of the complexes is in competition with the activation and resulted in precipitation of particulate Mo over time and explains the deactivation as observed in catalytic tests. The novel freeze-quench approach, which can trap reaction solutions within 1 s of mixing, opens up a large field of homogeneous catalysis and liquid chemistry to be studied, being able to quench this rapidly, whilst characterisation techniques with long data acquisition can be performed.

© 2011 Published by Elsevier Inc.

1. Introduction

The efficient catalytic conversion of small molecules into more complex species in commercial demand continues to be a very important feature of the global chemical industry, and the ability to increase the specificity and selectivity of these processes is essential for clean, energy efficient processes. Oligomerisation of alkenes usually occurs via transition metal or aluminium catalysed processes to produce mixtures of alkenes in the C_4 – C_{26} range [1,2]. However, the selective trimerisation and tetramerisation of ethene to produce the linear α -olefins (LAOs) 1-hexene and 1-octene, respectively, are of major significance due to the importance of these co-monomers in the production of linear low-density polyethylene (LLDPE) [2–4]. LLDPE accounts for around 50% of the LAO co-monomers produced industrially. A variety of transition metal catalysts facilitate the selective trimerisation of ethene, most of which are based on early transition metals such as titanium, tantalum or, most importantly, chromium [2–4]. These form the basis of several key industrial catalysts, including the Phillips pyrrolide system, the Sasol mixed heteroatom systems and the BP diphosphine systems [5–7].

The extremely high selectivity for 1-hexene is thought to occur via a mechanism based upon a metallocyclic intermediate formed through the reaction of Cr(III) pre-catalysts with ethene in the presence of methylaluminoxane (MAO) co-catalyst [2,6,8]. The auxiliary ligand on Cr(III) is generally a tridentate ligand incorporating Group 15 or 16 donor atoms, e.g. $[\text{CrCl}_3(\text{SNS})]$ ($\text{SNS} = \text{RS}(\text{CH}_2)_2\text{NH}(\text{CH}_2)_2\text{SR}$) and $[\text{CrCl}_3\{\text{R}_2\text{P}(\text{CH}_2)_2\text{NH}(\text{CH}_2)_2\text{PR}_2\}]$ ($\text{R} =$ long-chain alkyl group). Chromium complexes containing the ligand $\text{Ph}_2\text{PN}(\text{iPr})\text{PPh}_2$ (PNP) are highly selective catalyst precursors for the tetramerisation of ethylene to 1-octene when activated with MAO, and improved activities are achieved when aluminate or BARF activators are introduced [9–11]. The pursuit of catalysts with ever higher specificities and selectivities for these oligomerisations and polymerisations demands a detailed understanding of the individual stages of the catalytic cycle, the dependence upon metal, promoter and/or co-catalyst. However, developing such catalyst systems is hindered by characterisation difficulties due to the paramagnetism of the majority of the Cr complexes (precluding NMR analysis), and since MAO is not a single chemical entity, therefore its precise role is difficult to establish. The role of the ligand donor types (hard versus soft) and architectures are undoubtedly very important in defining the mechanisms in these processes, promoting different reaction pathways. Further, whilst Cr complexes with softer P/S donor atoms tend to lead to trimer/tetramer, the use of harder donor ligands only (e.g. amines) favours a Shultz–Flory distribution of oligomers [2].

* Corresponding author. Fax: +49 89 28912866.

E-mail address: moniek.tromp@tum.de (M. Tromp).

Work on the industrially important $[\text{CrCl}_3(\text{SNS})]$ with various alkylating agents by Gambarotta and co-workers suggests that at low Cr:Al ratios Cl-bridged dimers are formed, including $[\{(\text{SNS})\text{CrMe}\}_2(\mu\text{-Cl})_2]^{2+}$ [12]. Braunstein et al. have also recently shown that for the $[\text{CrCl}_3(\text{NPN})]$ (NPN = bis(2-picolyl)phenylphosphine) chloro-bridged dimers, as well as mononuclear clusters with a mixture of alkyl and halide ligands can be formed, depending on the alkylating agent and reaction conditions [13]. It is however important to note that the ratio of Cr:MMAO in the operating catalyst system is significantly higher than used in these studies.

Previously, we have examined a range of Cr(III) complexes with various neutral tridentate N-, S- and O-donor ligands comprised of three distinct architectures: facultative ($\text{S}(\text{CH}_2\text{CH}_2\text{SC}_{10}\text{H}_{21})_2$ (SSS-Decyl) and $\text{O}(\text{CH}_2\text{CH}_2\text{SC}_{10}\text{H}_{21})_2$ (SOS-Decyl), tripodal ($\text{MeC}(\text{CH}_2\text{SC}_4\text{H}_9)_3$, $\text{MeC}(\text{CH}_2\text{SC}_{10}\text{H}_{21})_3$) and macrocyclic ($\text{C}_{10}\text{H}_{21}_3[9]\text{aneN}_3$ ($[9]\text{aneN}_3 = 1,4,7\text{-triazacyclononane}$) as catalysts for olefin oligomerisation and polymerisation and probed the identity of the species before and after addition of the molecular alkylating agent, AlMe_3 , using IR, UV/visible and EPR spectroscopy along with X-ray Absorption Fine Structure (XAFS) studies [14]. Treatment of these complexes with excess (300 mol. equivs.) modified MAO (MMAO) leads to catalytically active species and shows significant dependence upon the ligand donor set. UV/visible and EPR measurements suggest that a change in the oxidation state of the chromium metal centre occurs in all these examples upon addition of excess AlMe_3 , lending support to the proposal that the catalysis involves a Cr(II)/Cr(IV) redox cycle. The partial structures of the AlMe_3 -activated species were probed via XAFS spectroscopy. It appears that when the Cr(III) complexes are treated with AlMe_3 , the Cl ligands are substituted by methyl groups and some ligands substantially dissociate from the metal centre; with the resulting species catalysing the oligomerisation and polymerisation of ethylene.

Whilst these are the first XAFS studies probing the activation of the Cr-based oligomerisation/polymerisation pre-catalysts, the timescale for the measurements (usually 2–4 h to acquire sufficient data from ~ 5 mM solutions – corresponding to the approximate Cr concentration in the operating catalyst – for partial structure analysis) mean that, by definition, these are ‘end-state’ investigations. The information that can be obtained from such measurements provides limited insight into the active species given that under the operating conditions the catalyst lifetime is typically < 1 h.

XAS (in energy dispersive mode (EDE)) was for the first time successfully synchronised with a stopped-flow experiment in 1990, in which the oxidation of Fe^{III} aq by hydroquinone was investigated [15]. More recently, stopped-flow systems have been developed for homogeneous catalysis studies, to probe homogeneous catalytic intermediates *in situ* and time-resolved (milliseconds) [16–18]. In the stopped-flow system, the evolution of the reaction mixture can be monitored in time with EDE or Quick-XAS (QEXAFS), allowing full Extended X-ray Absorption Fine Structure (EXAFS) spectra to be obtained in the millisecond to second timescale [19]. The problem with this set-up is that XAFS data acquisition in fluorescence mode is not possible (only transmission), and therefore, a relatively high concentration of the species under investigation is required. At the same time, the complete reaction mixture, i.e. including solvents and reagents, should not be too absorbing at the X-ray energies required for the experiment. The stopped-flow EDE method has been proven for homogeneous Pd¹⁶ and Re [20] systems with a high energy Pd K- and Re L-edge, enabling the *in situ* transmission experiments. However, although the method has been proven for homogeneous Ni (8.333 keV)¹⁶ and Cu (8.979 keV)¹⁸ systems, the Cr K-edge is at an even lower energy of 5.989 keV. Not only the solvent and reactant molecules, but even a few cm of air, are highly absorbing at these energies, severely hampering the transmission experiment.

We have pursued two methods to allow easier characterisation of these catalytic systems: (i) substituting the Cr(III) for the heavier 4d Mo(III) organometallic systems to model the early stages of the activation and (ii) modification of the stopped-flow system in order to maintain the advantages of the time resolution of the instrument, but also trapping the intermediates to allow long data acquisition via XAS to be conducted.

1.1. Mo(III) complexes

We have prepared the analogous Mo(III) trichloro complexes, $[\text{MoCl}_3(\text{L})]$ (L = SNS and SSS) and investigated their utility as stoichiometric model systems for the Cr catalysts by determining their reactivities with AlMe_3 . $[\text{MoCl}_3(\text{SNS-R})]$ complexes for a variety of R groups have been reported previously, although they show negligible catalytic activity towards ethene oligomerisation [21]. However, it is reasonable that the Mo systems might undergo similar chemistry in the early stages of activation, the slower kinetics at Mo will aid identification of individual species in the reaction. Furthermore, the Mo systems are also chosen as model systems because of the higher Mo K-edge energy at which the X-ray experiment can be undertaken and thus the increased time resolution of the XAS experiment to be obtained. Mo will allow time-resolved transmission studies in which real reaction intermediates are likely to be probed instead of the final (often decomposed) end-states of the Cr systems. With the Mo K-edge being present in the similar high energy range of Pd (i.e. ~ 20 keV)¹⁶ the potential of the stopped-flow EDE approach for these systems is high. In a further modification, the $[\text{MoBr}_3(\text{L})]$ analogues were also synthesised in order to aid distinction between the S of the ligand and the halide in the EXAFS analyses, which is not possible for S and Cl since they are corresponding neighbours in the periodic table with similar backscattering amplitudes.

1.2. Stopped-flow freeze-quench XAS development

In order to overcome the inherent obstacles associated with stopped-flow XAS studies, as mentioned, and to allow accurate characterisation of reaction intermediates, a XAFS cell that allows ‘trapping’ (stabilisation) of the intermediate species present at various stages of activation and catalysis reaction, by rapid quenching of the catalyst system is required. With the catalytic intermediate ‘trapped’, XAFS experimentation can subsequently be performed in fluorescence mode with long data acquisition times as required for low energy systems like Cr. The development of such a XAFS quench cell to allow highly reactive transients to be trapped on a sub-second timescale and analysed structurally and electronically will be complementary to the established stopped-flow EDE procedure, allowing in principle the in-depth study of any homogeneous process. This approach will provide detailed structural and electronic insights in homogeneous (catalytic) reaction mechanisms. Although freeze-quench (also in combination with stopped-flow methodologies) is used frequently for biological and bio-inorganic systems [22], this is a new approach in homogeneous catalysis and requires considerable modifications of the apparatus (*vide infra*).

Here, we report on the Mo(III) organometallic complexes and their activation with AlMe_3 , as well as a special quench-freeze XAFS cell designed to allow detailed XAFS and XANES studies to be performed to probe the early stages of activation and catalysis and thus provide a more detailed understanding of the activation stages of the polymerisation and oligomerisation catalyst systems rather than end-state studies. The results are shown for Mo systems, and their analogy to the Cr is made.

2. Experimental

2.1. Mo complex synthesis and characterisation

All complexes were synthesised under inert conditions using standard Schlenk line techniques, using dry solvents, having previously been distilled from appropriate drying agents. Complexes $[\text{MoCl}_3(\text{THF})_3]$ [23] and $[\text{MoBr}_3(\text{THF})_3]$ [24] and ligand $\text{HN}(\text{CH}_2\text{CH}_2\text{SC}_{10}\text{H}_{21})_2$ [25] were synthesised in accordance with previously published procedures. All metal complexes were stored under inert atmosphere in a glove box. AlMe_3 was purchased from Aldrich (2.0 M in hexanes) and titrated using the published procedure [26]. All solvents used in the stopped-flow instrument were purchased (anhydrous) from Aldrich and used as received.

^1H and $^{13}\text{C}\{^1\text{H}\}$ NMR spectra were recorded on a Bruker AV300 spectrometer. Micro-analyses were obtained through Medac Ltd., Egham UK. Infrared spectra were recorded as a Nujol mull between CsI plates under inert conditions, using Perkin Elmer FT-IR Spectrum 100 Spectrometer across the range 4000–200 cm^{-1} . Only the key bands associated with the NH function and the Mo–Cl stretching vibrations are quoted below. UV–visible spectra were recorded both using the stopped-flow instrument (Fibre optic J & M Analytic MCS–UVNIR) and using a Perkin Elmer Lambda 19 spectrometer either in solution in a 1-cm path-length quartz cuvette, or as solids by diffuse reflectance (DR). All spectroscopic samples were prepared freshly in a dry N_2 -purged glove box.

2.1.1. $S(\text{CH}_2\text{CH}_2\text{SCH}_2\text{-C}_6\text{H}_4\text{-p-C}(\text{CH}_3)_3)_2$ [SBZ]

Sodium (2.67 g, 116.3 mmol) was slowly dissolved in a solution of ethanol (200 mL) and bis(2-mercaptoethyl)sulphide (7.16 g, 46.40 mmol) under an N_2 atmosphere. The solution was heated to reflux and turned cloudy upon the dropwise addition of 4-tert-butylbenzylbromide (21.36 g, 94.03 mmol); this was then refluxed overnight under N_2 . Ethanol was removed *in vacuo*, and the reaction was hydrolysed using water (50 mL). After extraction with diethyl ether (3×30 mL), the organics were combined, dried over MgSO_4 , filtered and the solvent removed *in vacuo*. The yellow oil was further dried under vacuum. Yield: 18.15 g, 40.6 mmol (88%). ^1H NMR – ppm (CD_2Cl_2): 1.32 (s, [18H], CH_3), 2.63 (m, [8H], CH_2S), 3.72 (s, [4H], $\text{C}_6\text{H}_4\text{-CH}_2\text{S}$), 7.2, 7.4 (dd, [8H], Ar). $^{13}\text{C}\{^1\text{H}\}$ NMR – ppm (CD_2Cl_2): 31.7 (CH_3), 32.1, 32.5 (CH_2S), 36.4 ($\text{C}_6\text{H}_4\text{-CH}_2\text{S}$), 126.0, 129.0 (ArCH), 135.8, 150.7 (ArC).

2.1.2. $[\text{MoCl}_3\{\text{HN}(\text{CH}_2\text{CH}_2\text{SC}(\text{CH}_3)_3)_2\}]$ [MoCl₃(SNS-^tBu)]

$\text{HN}(\text{CH}_2\text{CH}_2\text{SC}(\text{CH}_3)_3)_2$ (0.9 g, 3.6 mmol) was added directly to a suspension of $[\text{MoCl}_3(\text{THF})_3]$ (1.0 g, 2.4 mmol) in THF (15 mL), giving an orange solution after 2 h. This was then allowed to stir overnight under N_2 . The solution was filtered under N_2 and washed with cold CH_2Cl_2 (3×5 mL). The yellow solid was dried *in vacuo*. Yield: 0.7 g, 1.6 mmol (64%). DR UV/Vis Spectrum (CaF_2): λ_{max} 446 nm. IR (Nujol mull, cm^{-1}): 3144 (NH), 336s, 313s, 303s (Mo–Cl). Micro-analysis required for $\text{C}_{12}\text{H}_{27}\text{Cl}_3\text{MoNS}_2$: C = 31.9; H = 6.0; N = 3.1; found C = 32.4; H = 6.1; N = 2.6%.

2.1.3. $[\text{MoCl}_3\{\text{HN}(\text{CH}_2\text{CH}_2\text{SC}_{10}\text{H}_{21})_2\}]$ [MoCl₃(SNS-Decyl)]

$\text{HN}(\text{CH}_2\text{CH}_2\text{SC}_{10}\text{H}_{21})_2$ (1.4 g, 3.6 mmol) was added directly to a suspension of $[\text{MoCl}_3(\text{THF})_3]$ (1.0 g, 2.4 mmol) in THF (20 mL). The mixture was allowed to stir overnight under N_2 , giving a very dark solution. The THF was then reduced to 5 mL *in vacuo*, where CH_2Cl_2 (15 mL) was added and the mixture was allowed to stir for a further 14 h under N_2 . All the solvent was then removed *in vacuo*, and dry hexane added. The solution was stirred and sonicated, and the dark brown solid was then filtered under N_2 and dried *in vacuo*. Yield: 1.27 g, 2.1 mmol (86%). UV/Vis spectrum (toluene): λ_{max} 455 nm, $\epsilon = 350 \text{ mol}^{-1} \text{ dm}^3 \text{ cm}^{-1}$. IR (Nujol mull, cm^{-1}):

3158 (NH), 324br sh), 311s (Mo–Cl). Micro-analysis required for $\text{C}_{24}\text{H}_{51}\text{Cl}_3\text{MoNS}_2$: C = 46.5; H = 8.3; N = 2.3; found C = 46.6; H = 8.4; N = 2.5%.

2.1.4. $[\text{MoCl}_3\{S(\text{CH}_2\text{CH}_2\text{SCH}_2\text{-C}_6\text{H}_4\text{-p-C}(\text{CH}_3)_3)_2\}]$ [MoCl₃(SBz)]

$S(\text{CH}_2\text{CH}_2\text{SCH}_2\text{-C}_6\text{H}_4\text{-p-C}(\text{CH}_3)_3)_2$ (0.59 g, 1.31 mmol) was added directly to a suspension of $[\text{MoCl}_3(\text{THF})_3]$ (0.5 g, 1.19 mmol) in THF (20 mL). The solution was allowed to stir for 3 d. under N_2 to give a very dark solution. The solvent was then removed *in vacuo* to give a very dark solid. Dry hexane (25 mL) was added and the solution was allowed to stir for 30 min. The red solid was then filtered under N_2 and dried *in vacuo*. Yield: 0.56 g, 0.86 mmol (72%). UV/Vis spectrum (toluene): λ_{max} 476 nm, $\epsilon = 938 \text{ mol}^{-1} \text{ dm}^3 \text{ cm}^{-1}$. IR (Nujol mull, cm^{-1}): 367 m, 352sh, 322s (Mo–Cl). Micro-analysis required for $\text{C}_{26}\text{H}_{38}\text{Cl}_3\text{MoS}_3$: C = 48.1; H = 5.9; found C = 47.8; H = 5.8%.

2.1.5. $[\text{MoBr}_3\{\text{HN}(\text{CH}_2\text{CH}_2\text{SC}_{10}\text{H}_{21})_2\}]$ [MoBr₃(SNS-Decyl)]

Prepared in the same manner as $[\text{MoCl}_3(\text{SNS-}^t\text{Bu})]$ above, using $[\text{MoBr}_3(\text{THF})_3]$ (0.6 g, 1.09 mmol) and $\text{HN}(\text{CH}_2\text{CH}_2\text{SC}_{10}\text{H}_{21})_2$ (0.55 g, 1.31 mmol), with 1.5 d. stirring after the addition of CH_2Cl_2 . UV/Vis spectrum (CH_2Cl_2): λ_{max} 486 nm (sh), $\epsilon = 1000$; 421 nm, $\epsilon = 1625 \text{ mol}^{-1} \text{ dm}^3 \text{ cm}^{-1}$. IR (Nujol mull, cm^{-1}): 3172 (NH), 257 m, 243sh, 228 m (Mo–Br). Micro-analysis required for $\text{C}_{24}\text{H}_{51}\text{Br}_3\text{MoNS}_2$: C = 38.3; H = 6.8; N = 1.9; found C = 39.0; H = 7.2; N = 2.0%.

2.1.6. $[\text{MoBr}_3\{S(\text{CH}_2\text{CH}_2\text{SCH}_2\text{-C}_6\text{H}_4\text{-p-C}(\text{CH}_3)_3)_2\}]$ [MoBr₃(SBz)]

$S(\text{CH}_2\text{CH}_2\text{SCH}_2\text{-C}_6\text{H}_4\text{-p-C}(\text{CH}_3)_3)_2$ (0.49 g, 1.09 mmol) was added directly to a suspension of $[\text{MoBr}_3(\text{THF})_3]$ (0.5 g, 0.91 mmol) in THF (10 mL). The solution was allowed to stir for 1 d. under N_2 to give an orange precipitate. The solvent was then removed *in vacuo* and CH_2Cl_2 added to the orange solid to ensure all starting material had dissolved. This was allowed to stir overnight and then filtered under N_2 . The orange solid was then washed with further CH_2Cl_2 , filtered under N_2 and dried *in vacuo*. Yield: 0.38 g, 0.49 mmol (54%). UV/Vis spectrum (toluene): λ_{max} 472 nm, $\epsilon = 2300 \text{ mol}^{-1} \text{ dm}^3 \text{ cm}^{-1}$. IR (Nujol mull, cm^{-1}): 287 m, 273 m, 265 m (Mo–Br). Micro-analysis required for $\text{C}_{26}\text{H}_{38}\text{Br}_3\text{MoS}_3$: C = 39.9; H = 4.9; found C = 40.1; H = 4.8%.

2.1.7. $[\text{MoCl}_3\{[9]\text{aneS}_3\}]$ ([9]aneS₃ = 1,4,7-trithiacyclononane)

Prepared by a modification of the literature method [27]. [9]aneS₃ (0.1 g, 0.6 mmol) in THF (5 mL) was added to $[\text{MoCl}_3(\text{THF})_3]$ (0.2 g, 0.6 mmol) in THF (5 mL). This was allowed to stir for 2 h at room temperature to give a cloudy red solution. The solvent was then reduced to ~2 mL *in vacuo*, and CH_2Cl_2 (20 mL) added. The reaction was left to stir overnight. The red precipitate was then filtered, washed with CH_2Cl_2 (2×5 mL) and dried *in vacuo* to give an orange solid. Yield: 0.10 g, 0.26 mmol (48%). DR UV/Vis spectrum (BaSO_4): 480 nm. IR (Nujol mull, cm^{-1}): 315s, 292 m (Mo–Cl). Micro-analysis required for $\text{C}_6\text{H}_{12}\text{Cl}_3\text{MoS}_3$: C = 18.8; H = 3.2; found C = 19.1; H = 3.1%.

2.2. X-Ray crystallography

Details of the crystallographic data collection and refinement parameters are given in Table 1. Crystals of $[\text{MoCl}_3\{[9]\text{aneS}_3\}]$ and weakly diffracting crystals of $[\text{MoCl}_3\{^t\text{BuS}(\text{CH}_2)_2\text{NH}(\text{CH}_2)_2\text{S}^t\text{Bu}\}]$ suitable for single crystal X-ray analysis were obtained from a solution of the complex in THF or CH_2Cl_2 solution (at -18°C), respectively. Data collections used a Bruker–Nonius Kappa CCD diffractometer fitted with monochromated Mo $\text{K}\alpha$ radiation ($\lambda = 0.71073 \text{ \AA}$), with the crystals held at 120 K in a nitrogen gas stream. Structure solution and refinement were straightforward [28]. H atoms bonded to C were introduced into the models in idealised positions using the default C–H distance. The crystal

Table 1
Crystal data and structure refinement details^a.

Compound	[MoCl ₃ ([9]aneS ₃)]	[MoCl ₃ { ^t BuS(CH ₂) ₂ NH(CH ₂) ₂ S ^t Bu}]
Formula	C ₆ H ₁₂ Cl ₃ MoS ₃	C ₁₂ H ₂₇ Cl ₃ MoNS ₂
<i>M</i>	382.63	451.76
Crystal system	Tetragonal	Orthorhombic
Space group (no.)	I4 ₁ cd (110)	P2 ₁ 2 ₁ 2 ₁ (19)
<i>a</i> (Å)	17.213(2)	6.890(2)
<i>b</i> (Å)	17.213(2)	9.349(3)
<i>c</i> (Å)	16.389(2)	30.338(9)
α (°)	90	90
β (°)	90	90
γ (°)	90	90
<i>U</i> (Å ³)	4855.7(10)	1954.3(10)
<i>Z</i>	16	4
μ (Mo Kα)/mm ⁻¹	2.210	1.284
Total no. reflections	16,285	22,151
Unique reflections	2579	3826
<i>R</i> _{int}	0.0938	0.170
No. of parameters, restraints	118, 1	173, 24
Goodness-of-fit on <i>F</i> ²	1.116	1.112
<i>R</i> ₁ ^b [<i>I</i> _o > 2σ(<i>I</i> _o)]	0.050	0.101
<i>R</i> ₁ (all data)	0.069	0.129
<i>wR</i> ₂ ^b [<i>I</i> _o > 2σ(<i>I</i> _o)]	0.089	0.2219
<i>wR</i> ₂ (all data)	0.097	0.237

^a Common items: temperature = 120 K; wavelength (Mo Kα) = 0.71073 Å; θ(max) = 27.5°.

^b $R_1 = \sum ||F_o| - |F_c|| / \sum |F_o|$. $wR_2 = [\sum w(F_o^2 - F_c^2)^2 / \sum wF_o^4]^{1/2}$.

quality for [MoCl₃{^tBuS(CH₂)₂NH(CH₂)₂S^tBu}] was modest, and hence structure determination is of modest quality, although the core geometry and isomer determination are not in doubt, detailed comparisons of the geometric parameters should be treated with care. The structures are shown in Figs. 1 and 2. Selected bond lengths and angles are presented in Tables 2 and 3. CIF files of the crystal structure data are available as Electronic Supplementary Data files.

2.3. XAFS cell development

We have developed a freeze-quench (FQ) XAFS cell to permit measurements to be made following rapid quenching of the catalyst mixture. This is essential in order to be able to probe the early stages of activation and catalysis in the true trimerisation and tetramerisation mixtures and to provide a more detailed understand-

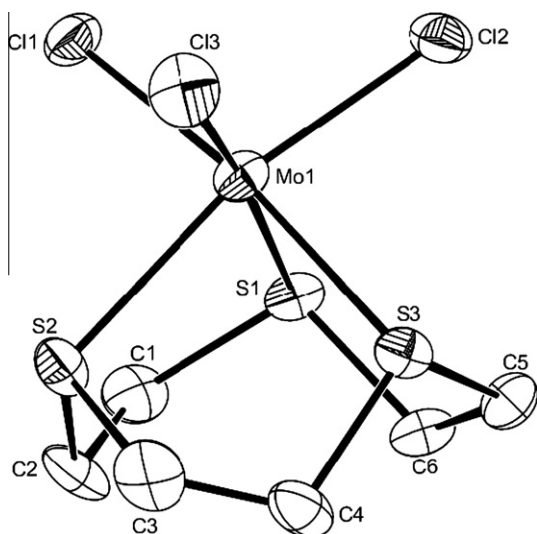


Fig. 1. View of the structure of [MoCl₃([9]aneS₃)] with number scheme adopted. H atoms are omitted for clarity and ellipsoids are drawn at the 50% probability level.

ing of individual stages of the cycle(s). The stopped-flow system has a proven performance in controlled and reproducible injection of accurate mixtures in millisecond timescales. Therefore, the set-up as developed here is based on the stopped-flow EDE approach, using a commercially available stopped-flow system with a proven performance for combined EDE/UV–Vis experimentation [16,18].

The stopped-flow (SFM400/QS, Biologic, France) consists of four syringes that can be filled with reaction solution or solvent [18,29]. The system is computer controlled and allows injection of very precise volumes with controlled injection rates (and thus injection times). The solutions are injected using stepper motors via the delay lines and the mixers into a cuvette or capillary, depending on the requirement. Specially designed quartz cuvettes allow time-resolved EDE experiments to be performed on the injected mixtures. Using cuvettes with two transmission pathways perpendicular to each other will allow the addition of a complementary technique, like UV/Vis, to be performed simultaneously [18]. An optical fibre UV/Vis spectrometer (MCS–UV–VIS–NIR 1/500-3 Fast Diode Array Detector, BioLogic, France), specially customised for the stopped-flow, is also used in this study. The UV–Vis technique is used to perform time-resolved UV/Vis studies (in the laboratory) as well as combined EDE/UV/Vis experiments (at the synchrotron). Due to the air and moisture sensitive nature of the chemistry, the entire stopped-flow is connected to a Schlenk line allowing us to work under an argon atmosphere. To ensure the stopped-flow is completely air and moisture free, a careful cleaning and passivating procedure is employed before every experiment. The internal components of the stopped-flow instrument were manufactured in Kelf[®] (polychlorotrifluoroethylene), with Kalrez[®] (perfluoroelastomer) rings, to ensure full chemical compatibility.

The standard freeze-quench accessory as available from Biologic was developed for non-sensitive water solution, spraying through air into isopentane. Because of the air and moisture sensitivity or our chemistry, this was not a viable option. Therefore, we have developed a XAFS measurement cell with freeze-quench system to be attached to the stopped-flow, Fig. 3. A Kapton[®] capillary is mounted into a custom holder attached to the standard Biologic freeze-quench accessory. The holder allows direct injection into the Kapton[®] tube whilst an argon gas is flowed around the spray exit and tube inlet and prevents ingress of air (or moisture) into

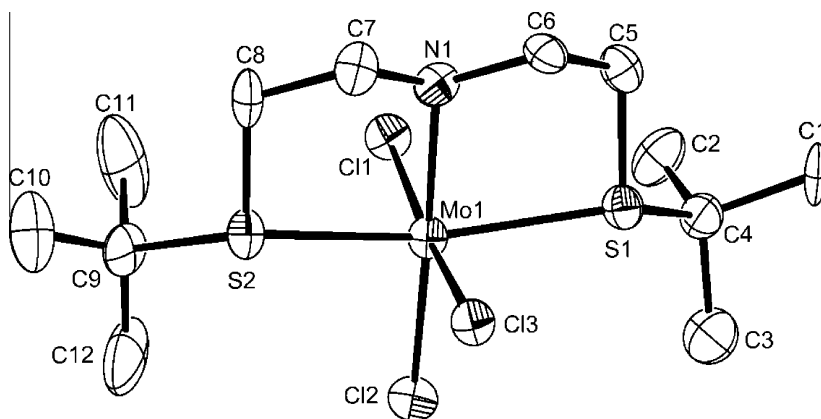


Fig. 2. View of the structure of $[\text{MoCl}_3\{\text{tBuS}(\text{CH}_2)_2\text{NH}(\text{CH}_2)_2\text{S}^t\text{Bu}\}]$ with number scheme adopted. H atoms are omitted for clarity and ellipsoids are drawn at the 50% probability level.

Table 2

Selected bond lengths (Å) and angles (°) for $[\text{MoCl}_3\{(\text{9})\text{aneS}_3\}]$.

Mo1–Cl1	2.402(2)	Mo1–Cl2	2.345(2)
Mo1–Cl3	2.385(2)	Mo1–S1	2.464(2)
Mo1–S2	2.520(2)	Mo1–S3	2.484(2)
Cl2–Mo1–Cl3	96.78(9)	Cl2–Mo1–Cl1	99.53(8)
Cl3–Mo1–Cl1	96.57(9)	Cl2–Mo1–S1	88.60(8)
Cl3–Mo1–S1	172.42(9)	Cl1–Mo1–S1	87.77(7)
Cl2–Mo1–S3	86.12(7)	Cl3–Mo1–S3	91.41(9)
Cl1–Mo1–S3	169.58(8)	S1–Mo1–S3	83.60(7)
Cl2–Mo1–S2	168.16(7)	Cl3–Mo1–S2	89.60(9)
Cl1–Mo1–S2	89.59(7)	S1–Mo1–S2	84.20(8)
S2–Mo1–S3	83.76(6)		

Table 3

Selected bond lengths (Å) and angles (°) for $[\text{MoCl}_3\{\text{tBuS}(\text{CH}_2)_2\text{NH}(\text{CH}_2)_2\text{S}^t\text{Bu}\}]$.

Mo1–N1	2.208(12)	Mo1–Cl1	2.384(4)
Mo1–Cl2	2.410(4)	Mo1–Cl3	2.452(4)
Mo1–S1	2.521(4)	Mo1–S2	2.532(4)
N1–Mo1–Cl1	85.2(3)	N1–Mo1–Cl2	176.4(3)
Cl1–Mo1–Cl2	91.28(13)	N1–Mo1–Cl3	88.5(3)
Cl1–Mo1–Cl3	173.66(14)	Cl2–Mo1–Cl3	95.01(13)
N1–Mo1–S1	80.0(3)	Cl1–Mo1–S1	95.90(13)
Cl2–Mo1–S1	101.14(13)	Cl3–Mo1–S1	82.06(12)
N1–Mo1–S2	81.2(3)	Cl1–Mo1–S2	96.92(13)
Cl2–Mo1–S2	98.46(13)	Cl3–Mo1–S2	83.02(12)
S1	Mo1	S2	156.26(12)

the sample. The Kapton[®] tube is sealed with a plug, and immersed into liquid nitrogen in a Dewar (before and during injection). As such the reaction mixture can be injected (collected) and frozen directly and maintained at 77 K. The injection and freezing time was estimated to be below 1 s. Different delays in the stopped-flow allow the accurate timing of reaction intermediates. For XAS experimentation, the tube with frozen sample is subsequently placed into a holder in the X-ray beam, whilst being cooled continuously using a Cryostream (100 K). By setting up the appropriate cryo flow rate, ice formation on the outside of the capillary is restricted (this is not crucial for the high energy Mo XAS data as obtained in this study, but will be when looking at low energy systems like the 3d transition metals with much lower X-ray edge energies).

The total set-up thus consists of different parts that can be used independently or as an ensemble. As such, the system is very versatile and allows a broad range of experiments to be performed; reactions at variable temperatures, direct time-resolved studies or via quench-freeze methods (from any given reaction temperature) allowing long data acquisition times (also non-XAS) if required.

2.4. XAFS experimentation

All samples for solid state Mo K-edge EXAFS analysis were mixed with boron nitride, pressed into pellets under inert atmosphere and encapsulated in Kapton[®] tape. All solution data collected for Mo K-edge EXAFS were obtained from solutions made up to the stated concentrations with anhydrous toluene under inert conditions. The solution was then transferred to a dry, argon-purged and sealed liquid XAFS cell [14] for analysis on the beamline. Reactions were also performed in this liquid XAFS cell by adding of the stated amount of AlMe_3 (2.0 M in hexane) (using a syringe) directly into the XAFS cell. The solution was then analysed with Mo K-edge EXAFS after ca. 5 min of reaction. In the rest of this paper, this cell is referred to as 'large solution cell' (in which we have measured reaction 'start- and end-states').

All stopped-flow and freeze-quench experiments were carried out using a BioLogic SFM-400 stopped-flow instrument as explained above. In stopped-flow mode, all reactions were observed in cuvette TC-100/10T with minimum dead volume of 30.2 μL . In time UV/Vis was collected using J and M Analytic AG MCS-UVNIR 500-3 fibre optic diode array spectrometer. When using the freeze-quench attachment, the same set-up is used (with UV-Vis and cuvette head removed) giving a total minimum dead volume of 19 μL from mixing to ejection, freezing time in toluene less than 1 s. Prior to all reactions using the stopped-flow instrument, the whole instrument was purged with argon, maintaining a positive pressure throughout (including waste lines) by attachment to a Schlenk line. All lines were washed with anhydrous toluene, then the subsequent reactant, followed by further washing with anhydrous toluene.

The Mo K-edge XAFS measurements were performed at different synchrotrons across Europe. Solid and solution (large solution cell) preliminary experiments were performed at BM26 (DUBBLE) [30] of the European Synchrotron Radiation Facility (ESRF) in Grenoble, France. Mo K-edge XAS data were obtained using a Si(111) double crystal monochromator using ionisation chambers for transmission detection, with acquisition times of 30 min (three scans were averaged to improve S/N unless stated otherwise). Solid and solution (large cell) experiments, as well as time-resolved stopped-flow QEXAFS/UV/Vis were performed at the SuperXAS beamline at the Swiss Light Source in Villigen, Switzerland. The time-resolved Mo K-edge QEXAFS experiments were performed using a fast scanning Si(111) double crystal monochromator, with a time resolution of 1 min/spectrum for the stopped-flow and 3 min/spectrum for the solids and large solution cells. All data from these experiments were obtained in transmission mode using

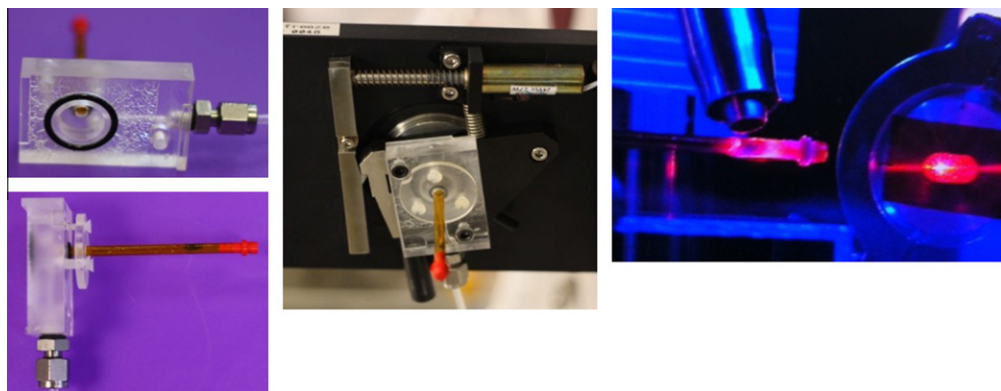


Fig. 3. Stopped-flow Freeze-Quench accessory: A Perspex box is constructed to be mounted to the standard spray outlet of the stopped-flow quench accessory and to hold the Kapton[®] tube. A gas inlet and outlet provide an argon gas atmosphere from the spray exit to the tube inlet. The right picture shows the Kapton[®] tube, containing frozen Mo intermediate, positioned in the X-ray beam using a red laser whilst in the cryostream.

ionisation chambers. Time-resolved QEXAFS/UV-Vis as well as freeze-quench experiments were performed at the B18 beamline [31] at Diamond Light Source in Didcot, England. A Si(111) double crystal was used in combination with ion chamber detectors for time-resolved transmission data and an Ortec[®] Ge 9 element Solid State detector for fluorescence acquisition on the frozen samples. Mo K-edge step-scans were obtained in 35 min, whereas the QEXAFS data were obtained with a time resolution of 30 s per spectrum. The time-resolved spectra shown in this paper are a combination of data obtained at the SLS and Diamond. All spectra were calibrated using a Mo foil. XAS data processing and EXAFS analysis were performed using IFEFFIT [32] with the Horae package [33] (Athena and Artemis). The amplitude, i.e. s_0^2 , was derived from EXAFS data analysis of known Mo reference compounds (with known coordination numbers which were fixed during analysis) to be 0.85, which was used as a fixed input parameter in all fits to allow coordination number (CN) refinement. The organometallic complexes were fitted using single crystal models or similar complexes, as indicated. The detailed fitting parameters are given in the results section.

The XANES data are not discussed in this paper. Because of the focus of the experiment onto obtaining time-resolved EXAFS at the best quality possible, the XANES data were obtained at relatively low resolution. Moreover, the changes in the XANES of the Mo K-edge are very small because of the broad edge at these high X-ray energies (long core hole lifetimes), which makes the differences between Mo³⁺, and potentially formed Mo²⁺ or Mo⁴⁺ very difficult to observe, especially since the K-edge reflects the dipole allowed $1s \rightarrow 5p$ transition and only probes the 4d states indirectly.

3. Results and discussion

3.1. Solid state and solution complexes

A series of Mo(III) complexes were successfully synthesised and characterised with standard techniques like IR and UV-Vis spectroscopy and micro-analysis (see Section 2): [MoCl₃{HN(CH₂CH₂SC₁₀H₂₁)₂}] [MoCl₃(SNS-Decyl)], [MoCl₃(SNS-tBu)], [MoCl₃{S(CH₂CH₂SCH₂-C₆H₄-*p*-C(CH₃)₃)₂}] [MoCl₃(SBz)], [MoBr₃{S(CH₂CH₂SCH₂-C₆H₄-*p*-C(CH₃)₃)₂}] [MoBr₃(SBz)] and [MoCl₃([9]aneS₃)] [9]aneS₃ = 1,4,7-trithiacyclononane. Only for the [MoCl₃(SNS-tBu)] and the [MoCl₃([9]aneS₃)] complexes were crystal structures obtained, so the structures of all complexes in the solid state and solution were carefully analysed to confirm their integrity and provide good starting points for the reaction studied.

The solid and solution structures of the complexes were confirmed by EXAFS and compared to the other characterisation obtained. The Mo K-edge EXAFS results of the chloride complexes [MoCl₃(SNS-Decyl)] and [MoCl₃(SBz)] are presented in Tables 4 and 5, and the Mo K-edge EXAFS results on the bromide analogue [MoBr₃(SBz)] in Table 6. Good fits have been obtained for all data sets, with low R-factors. Representative EXAFS data and fits are presented in Fig. 4, for [MoBr₃(SBz)] solid and solution. Some parameters with higher errors or Debye Waller factors are obtained and discussed when they appear.

The *mer*-[MoCl₃(SNS-Decyl)] complex was characterised by three chlorine atoms at 2.41(3) Å, two sulphurs at 2.50(2) Å and one nitrogen atom at ~2.1(1) Å. The crystal structure data of the *t*Bu-analogue, *mer*-[MoCl₃(SNS-*t*Bu)] (Tables 1 and 3), were used as an input model for the fit. The contribution of the nitrogen atom directly bonded to the Mo is very weak and difficult to identify, with a large error in distance and a large Debye Waller factor, due to the presence of the 5 higher Z sulphur and chlorine atoms. The contribution can be omitted and a good fit is obtained, however, crystal structure data (Mo-N 2.208(12) Å based on XRD – see Table 3) on the [MoCl₃(SNS-*t*Bu)] and IR results (via ν_{NH}) confirm its presence and thus a fixed coordination of one Mo-N is included in the fits. Because of the proximity of chlorine and sulphur in the periodic table, they cannot be distinguished based on EXAFS only. Their different assignment here was based on chemical knowledge on these compounds. The coordination numbers were fixed to simplify the fit and allow us to distinguish between the two shells.

The Mo-Cl distance of 2.41 Å corresponds well with an average of the three distances as observed in the [MoCl₃(SNS-*t*Bu)] crystal

Table 4

Mo K-edge EXAFS data analyses results on MoCl₃(SNS-Decyl) complex (all fitted in combined k^{1-3} -weighting).

Abs Sc	CN	R (Å)	$2\sigma^2(\text{Å}^{-2})$	Fitting parameters, k (Å ⁻¹)
<i>Solid</i> [MoCl ₃ (SNS-Decyl)]				
Mo-N	1 (fix)	2.1(1)	0.010(6)	2.0 < k < 14.7; 1.1 < R < 2.57 Amp = 0.85; E_0 = 3(1); R = 0.01
Mo-Cl(S)	3 (fix)	2.41(3)	0.002(3)	
Mo-S(Cl)	2 (fix)	2.50(2)	0.001(2)	
<i>Solution</i> [MoCl ₃ (SNS-Decyl)]				
Mo-N	1 (fix)	2.1(1)	0.015(9)	2.0 < k < 15.7; 1.1 < R < 2.7 Amp = 0.85; E_0 = 3(1); R = 0.02
Mo-Cl(S)	3 (fix)	2.40(2)	0.002(1)	
Mo-S(Cl)	2 (fix)	2.53(2)	0.002(2)	
<i>[MoCl₃(SNS-Decyl)] + 20 equivalent AlMe₃ – large solution cell</i>				
Mo-N/C	3(1)	2.22(9)	0.010(9)	2.0 < k < 11; 1 < R < 3 Amp = 0.85; E_0 = 3(3); R = 0.05
Mo-S(Cl)	1.9(9)	2.50(3)	0.003(4)	

Table 5Mo K-edge EXAFS data analyses results on MoCl₃(SBz) complex (all fitted in combined k^{1–3}-weighting).

Abs Sc	CN	R (Å)	2σ ² (Å ⁻²)	Fitting parameters, k (Å ⁻¹)
<i>Solid [MoCl₃(SBz)]</i>				
Mo–Cl(S)	2.8(3)	2.40(2)	0.002(2)	2.0 < k < 16.8; 1 < R < 2.9
Mo–S(Cl)	2.8(3)	2.43(2)	0.003(3)	Amp = 0.85; E ₀ = 1(1); R = 0.01
<i>Solution [MoCl₃(SBz)]</i>				
Mo–Cl(S)	2.8(3)	2.39(2)	0.001(2)	2.95 < k < 16.5; 1 < R < 3
Mo–S(Cl)	2.8(3)	2.46(2)	0.003(3)	Amp = 0.85; E ₀ = 1(1); R = 0.02
<i>[MoCl₃(SBz)] + 8 equivalent AlMe₃ – stopped-flow ~4 min</i>				
Mo–S(Cl)	2.2(9)	2.55(1)	0.002(1)	2.0 < k < 14.6; 1 < R < 5.5
Mo–C	3.6(9)	2.26(1)	0.002(1)	Amp = 0.85; E ₀ = 6(1); R = 0.01
Mo–Mo	1.3(8)	2.97(3)	0.010(5)	
Mo–Mo	2(1)	4.36(5)	0.011(4)	
Mo–Mo	11(9)	5.18(7)	0.015(7)	
<i>[MoCl₃(SBz)] + 20 equivalent AlMe₃ – large solution cell</i>				
Mo–S(Cl)	2.5(5)	2.55(1)	0.005(2)	2.0 < k < 15.3; 1.1 < R < 2.67
Mo–C	2.6(4)	2.23(1)	0.001(1)	Amp = 0.85; E ₀ = 8(1); R = 0.03

structure (Mo–Cl 2.384(4), 2.410(4), 2.452(4)). The Mo–S distance as detected corresponds well to XRD (Mo–S 2.521(4), 2.532(4)). The [MoCl₃(SNS-Decyl)] complex was subsequently dissolved in toluene and characterised with Mo K-edge EXAFS. As can be seen

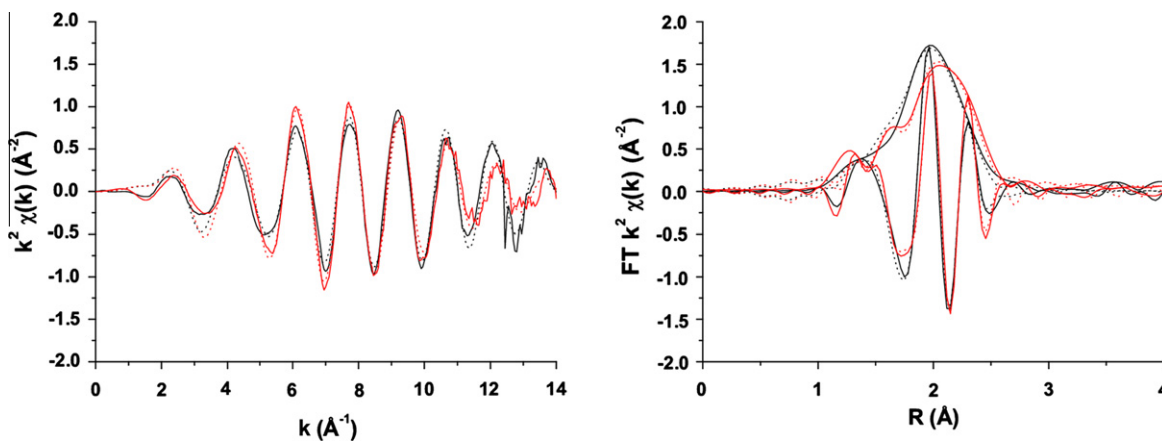
in Table 4, the results are similar to the solid state structure, as expected. Good fits have been obtained for solid state and solution, with low R-factors.

The solid state structure for the [MoCl₃(SBz)] complex was characterised with Mo K-edge EXAFS and its results presented in Table 5. The crystal structure of the [MoCl₃([9]aneS₃)] (see Tables 1 and 2) model compound was used as an input model for the fitting procedure. The structure of the [MoCl₃(SBz)] complex could be refined with three chlorine atoms at 2.40(2) Å and three sulphur at 2.43(2) Å, with low Debye Waller factors. The two shell analysis is consistent with a *facial* geometry as observed in the single crystal XRD for the [MoBr₃(SBz)] (vide infra). The obtained distances are in the range expected Mo–Cl 2.345(2), 2.385(2), 2.402(2) and Mo–S 2.464(2), 2.4838(19), 2.520(2) Å for [MoCl₃([9]aneS₃)]. Again, the structure in solution is similar to the solid state structure, as expected.

Table 6 presents the Mo K-edge EXAFS analyses results of the bromide analogue, i.e. [MoBr₃(SBz)]. Two shells can be refined for the solid state structure; one Mo–Br shell with a coordination number 2.5(9) and a distance of 2.54(2) Å and a low Debye Waller factor, and a second shell with 3.5(9) sulphur atoms at 2.45(6) Å with a large Debye Waller factor (0.010(6)). Whilst crystallographic data collected on a poorly diffracting crystal of [MoBr₃(SBz)] were not of sufficient quality for an accurate structure

Table 6Mo K-edge EXAFS data analyses results on MoBr₃(SBz) complex (all fitted in combined k^{1–3}-weighting).

Abs Sc	CN	R (Å)	2σ ² (Å ⁻²)	Fitting parameters, k (Å ⁻¹)
<i>Solid [MoBr₃(SBz)]</i>				
Mo–S	3.5(9)	2.45(6)	0.010(6)	1.7 < k < 14.2; 1.2 < R < 2.6
Mo–Br	2.5(9)	2.54(2)	0.002(3)	Amp = 0.85; E ₀ = -4(1); R = 0.007
<i>Solution [MoBr₃(SBz)]</i>				
Mo–S	3(fix)	2.45(2)	0.003(1)	1.8 < k < 13.5; 1.1 < R < 3
Mo–Br	3(fix)	2.55(1)	0.006(1)	Amp = 0.85; E ₀ = -4(1); R = 0.01
<i>[MoBr₃(SBz)] + 20 equivalent AlMe₃ – stopped-flow – after ~4 min</i>				
Mo–S	2.5(3)	2.45(1)	0.003(1)	2 < k < 17; 1.1 < R < 3
Mo–Br	1.4(9)	2.59(1)	0.006(4)	Amp = 0.85; E ₀ = -4(1); R = 0.01
<i>[MoBr₃(SBz)] + 20 equivalent AlMe₃ – stopped-flow – freeze-quench – after ~5 s</i>				
Mo–S	2.9(4)	2.41(1)	0.004(3)	2 < k < 14; 1 < R < 3
Mo–Br	2.4(7)	2.58(1)	0.005(3)	Amp = 0.85; E ₀ = -5(1); R = 0.01
<i>[MoBr₃(SBz)] + 20 equivalent AlMe₃ – stopped-flow – freeze-quench – after ~5 min</i>				
Mo–S	3.3(3)	2.38(1)	0.005(2)	2 < k < 14; 1 < R < 3
Mo–Br	1.6(8)	2.61(1)	0.005(3)	Amp = 0.85; E ₀ = -5(1); R = 0.01
<i>[MoBr₃(SBz)] + 20 equivalent AlMe₃ – large solution cell</i>				
Mo–S	2.8(5)	2.43(2)	0.003(2)	2 < k < 13; 1 < R < 3
Mo–Br	0.8(1)	2.61(2)	0.003(7)	Amp = 0.85; E ₀ = -4(2); R = 0.01

**Fig. 4.** Mo K-edge k²-weighted EXAFS and Fourier transform data (solid lines) and fits (dotted lines) for [MoBr₃(SBz)] solid (black) and solution (red).

determination, it did establish that the complex adopts the *fac*-isomer. The *fac* assignment is also consistent with observations on Cr(III) and other transition metal complexes with ligands containing $-\text{SCH}_2\text{CH}_2\text{SCH}_2\text{CH}_2\text{S}-$ linkages [34]. With Br being a stronger scatterer the shell with three Mo–Br contributions strongly dictates the overall fit. The Mo–S shell is less well defined, indicating a possible distribution of Mo–S distances in the solid state structure, despite the facial geometry. The solution structure, however, seems much better defined with a similar refined structure, but now with low Debye Waller factors for both shells. Because of the somewhat lower data quality, the coordination numbers were fixed input parameters.

With the complex solutions being the starting points associated with activation of the complexes for any of the reactions to be discussed in the next part, either in the large solution cell or the stopped-flow, the solution EXAFS data at the start of any reaction in the cell or the stopped-flow cuvette were obtained and analysed. All solution structures were identical, independent of the observation cell.

3.2. 'End-state' analyses

The so-called end-states of the reactions, i.e. Mo(III) complex activated with AlMe_3 , were characterised in the large solution cells. The reactions were performed in this cell by injecting the required amount of AlMe_3 (solution in hexane or toluene) to the complex in toluene solution. The EXAFS data acquisition for all these systems starts about 5 min after injecting the AlMe_3 , with an overall acquisition time of 35 min. The reactions were also followed with on-the-fly XAS, acquisition of one spectrum per minute, and no further changes were observed in this period of time (5–35 min) in this cell. This indicates that a true reaction end-state has been reached and measured. At longer timescales (>1.5 h), a clear precipitation of Mo metal could be observed for all mixtures, indicating a second, irreversible, reaction taking place. These reaction solutions were carefully checked for X-ray beam damage, but no effects could be observed. The solutions undergo the same colour changes without exposure to the X-ray beam, and Mo precipitation is observed at the same timescale (see also in '3.3 Time-Resolved XAS (and UV/Vis)').

The EXAFS analyses results of the reaction end points are again represented in Tables 4–6. The **[MoCl₃(SNS-Decyl)]** complex was reacted with 20 equivalents of AlMe_3 . The EXAFS data can be refined to two shells, i.e. a contribution of 3(1) N/C neighbours at 2.22(9) Å and a Mo–S shell of 1.9(9) sulphurs at 2.50(3) Å. As with the solid state structure and solution, the Mo–N/C contribution is difficult to determine and has the highest inaccuracy (large error on coordination number and distance, with a large Debye Waller factor). The Mo–S shell is well defined. However, between the solution before reaction and after (i.e. end-state), a clear decrease in overall intensity in EXAFS can be observed which corresponds to the loss in chlorine ligands. The SNS ligand remains intact, which is confirmed by the presence of the Mo–S coordination at a distance similar to the solution structure, and the presence of a Mo–N/C coordination. The increase in Mo–N/C coordination number can be attributed to the replacement of the chloride ligands by methyl groups of the AlMe_3 . The coordination number is not very well defined 3 ± 1 , but to achieve a full coordination sphere around the Mo, a **[Mo(CH₃)₃(SNS-Decyl)]** complex is likely to be formed, with one neighbour being the N atom of the SNS ligand and three more neighbours corresponding to carbon from the AlMe_3 moiety (see Fig. 5). This 'activated' Mo structure is in agreement with analogous $[\text{CrCl}_3(\text{L})]$ complexes upon activation with AlMe_3 [14].

Activation of **[MoCl₃(SBz)]** with 20 equivalents of AlMe_3 (Table 5, Fig. 6) leads to a similar end-state-structure **[Mo(CH₃)₃(SBz)]** with 3 sulphur atoms at 2.55(1) Å and 3 carbon atoms at 2.23(1)

Å, indicating the neutral ligand remains intact and associated to the metal (40 min of reaction), whereas the chlorine is replaced by carbon (i.e. methyl groups) (see Fig. 5). In this case, a very good fit with low error and Debye Waller factors for both shells is obtained, now dealing with just one type of S and one type of C neighbour. The Mo–S distance is slightly longer compared to the structure before reaction, consistent with the increases *trans*-influence of Me versus chloride, the former being the much stronger σ -donor.

The Br₃ analogue, however, shows a slightly different behaviour. Upon reacting 10 equivalents of AlMe_3 with **[MoBr₃(SBz)]**, no reaction at all is observed for reactions times up to 1 h. Increasing the ratio Mo complex: AlMe_3 to 1:20 (as with the complexes above), significant changes in the EXAFS are observed, but much smaller than for the tri-chloride systems. Comparing the EXAFS of the complex before and after reaction shows a decrease in EXAFS intensity only in the region between $5 < k < 11 \text{ \AA}^{-1}$, which is exactly the region where the Mo–Br is most significant (Mo–Br EXAFS intensity peaks around $k = 8$, whereas the Mo–S contribution is high at low k and diminishes towards higher k -values). Refining the end-state EXAFS data lead to a good fit of two shells, one Mo–S with a coordination number of 2.8(5) and a Mo–Br with a coordination number of 0.8(1) (without a change in distances or Debye Waller factors compared to the solution structure). Upon reaction with AlMe_3 the **[MoBr₃(SBz)]** complex loses its halide ligand, but at a very different timescale than the chloride analogue, i.e. the X/Me exchange kinetics are much slower going from the chloride to the bromide ligand (Fig. 5). The mechanism, however, seems comparable to the halide being abstracted by the AlMe_3 activator. The overall coordination of Mo seems too low to be realistic, but no further shell could be introduced reliably (to improve the fit significantly). Although there are small changes in EXAFS visible at low k -values, which might indicate the introduction of a light scatterer (C/N), the quality of the data does not allow us to fit a reliable and significant Mo–C contribution here. It is possible that the Mo–C contribution is disordered (high Debye Waller factor) and therefore too low in intensity to be determined under the strong Mo–S and Mo–Br scatterers (with the quality of the data we have). Similarly, the inclusion of a Mo–Mo contribution, in search for either a direct bonded Mo dimer [35] or a halide-bridged dimer, which has been suggested in related literature [12,13], was unsuccessful and not significant based on the data as obtained, but cannot be excluded completely. We thus most likely have a formed a mononuclear mixed alkyl and halide species (Fig. 5), as was suggested before for selected Cr systems under specific conditions [13]. For all reactions, at longer timescales >1.5 h, the Mo K-edge XAS signal disappears completely and black precipitate is observed in the cell, indicating the formation of Mo metal (Mo–Mo contributions observed in time-resolved experiment, *via infra*).

3.3. Time-resolved XAS (and UV/Vis)

Time-resolved reactions were performed using the stopped-flow instrument. The time-resolved XAS experiments were performed in transmission, through the observation cuvette, with time-resolved UV/Vis taken simultaneously, using optical fibres in transmission perpendicular to the XAS observation. Because of the different sensitivity of the two techniques, the observation path-length of the XAS was 10 times the path-length of the UV-Vis. The effect of the X-ray beam on the solution was carefully checked by performing the reactions with and without X-ray beam and observing the time-resolved UV/Vis spectra. No changes in the time-resolved UV/Vis spectra were observed upon performing the reactions in the X-ray beam, suggesting we are genuinely looking at the chemical reaction taking place.

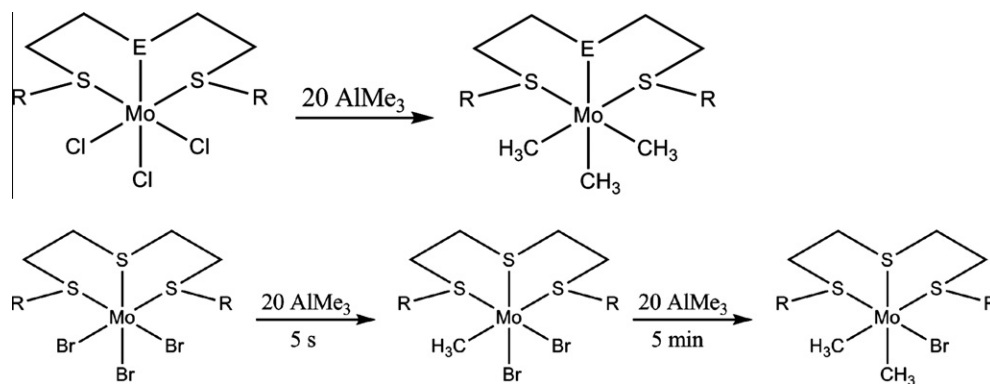


Fig. 5. Schematic representation of the proposed Mo complexes formed after activation with AlMe_3 ($\text{E} = \text{S}$ with $\text{R} = \text{CH}_2\text{-C}_6\text{H}_4\text{-p-C}(\text{CH}_3)_3$ or $\text{E} = \text{N}$ with $\text{R} = n\text{-C}_{10}\text{H}_{21}$).

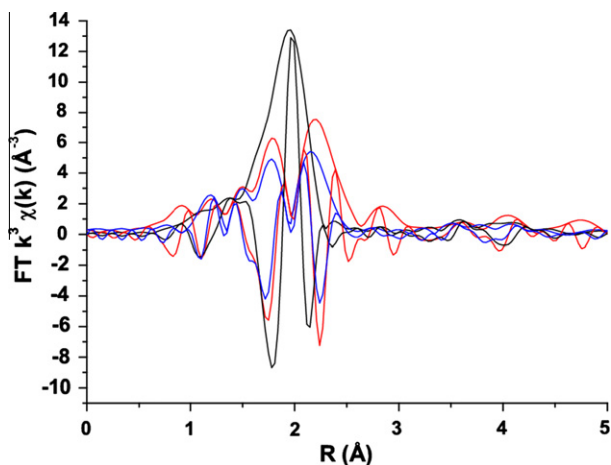


Fig. 6. Fourier transforms of k^3 -weighted EXAFS data on $[\text{MoCl}_3(\text{SBz})]$ (in solution, black line), with AlMe_3 in large solution cell (20 equivalents, ~ 40 min, blue line) and stopped-flow (8 equivalents, ~ 4 min, red line) ($2 < k < 16 \text{ \AA}^{-1}$). (For interpretation of the references to colour in this figure legend, the reader is referred to the web version of this article.)

The combined time-resolved data from the reaction of $[\text{MoCl}_3(\text{SNS})]$ (25 mM in toluene) with 20 equivalents of AlMe_3 (identical to the reaction performed in the large solution cell) are displayed in Fig. 7. QEXAFS spectra and time-resolved UV/Vis spectra shown here were obtained every 20 s. Because of the slow progress of the reaction and to enhance the clarity of the data and its changes, only a selection of spectra is presented here.

Although the overall EXAFS data quality is much lower (as expected due to the much shorter acquisition times), the overall change in EXAFS in time is clear and identical to the end-state solution as discussed above, i.e. an overall loss in EXAFS intensity indicating a loss of ligand. It is interesting to observe that most of the changes are happening in the first 1.5 min, which is confirmed by the UV/Vis data obtained simultaneously. The UV/Vis spectra of the Mo starting complexes each show the lowest band around $22,000 \text{ cm}^{-1}$, attributed to the $^4\text{A}_{2g}$ to $^4\text{T}_{2g}$ transition of a Mo(III) complex in approximately O_h symmetry. This corresponds to an increase in Dq of approximately 50% relative to the corresponding Cr(III) complexes [2,9,14,36], which is reasonable on the basis of their respective $4d^3$ and $3d^3$ configurations. Based on Jorgensen's model [37], the lowest energy charge transfer transitions are expected to occur $>30,000 \text{ cm}^{-1}$. Upon addition of AlMe_3 the d-d transition decreases in intensity, with concomitant appearance of new bands over a period of a few minutes (Fig. 7), and then disappearance of all bands occurring around 18 min. The combination of

the UV/Vis measurements with the EXAFS measurements is very useful in establishing when changes in speciation occur and hence guiding when EXAFS data should be recorded. After a reaction time of 18 min in the stopped-flow, the Mo K-edge XAS signal as well as the UV/Vis signal are lost completely, indicating the precipitation of Mo. It is interesting to note that the precipitation of Mo metal is observed at much shorter timescales compared to the dropout observed in the large solution cell (18 min compared to 1.5 h). This is probably due to the much smaller volume of the stopped-flow cuvette compared to the large cell (30 μL and 3 mL, respectively). The effects of X-ray beam were not significant as the same precipitation rates were observed when performing the reaction without the X-ray beam (which was checked for both the large solution cell and for the stopped-flow, as mentioned).

The reaction of $[\text{MoCl}_3(\text{SBz})]$ was also performed in the stopped-flow with different ratios of AlMe_3 and followed with QEXAFS (1 spectrum/min). When the reaction is performed at the high $\text{MoCl}_3(\text{SBz})$: AlMe_3 ratio of 1:20 as was performed in the large solution cell, the immediate precipitation of Mo was observed in the stopped-flow cuvette, hindering the spectroscopy. Lower amounts of AlMe_3 were therefore investigated. At a stoichiometric amount of $\text{MoCl}_3(\text{SBz})$: AlMe_3 of 1:1, no reaction was observed. When the amount of AlMe_3 was increased to 4 and 8 equivalents, changes in the EXAFS upon reaction were observed, at the same timescales. The EXAFS analysis of the 8 equivalent AlMe_3 data after 4 min of reaction is presented in Table 5. A full displacement of the chlorine ligand by carbon is observed, as for the end-state measure in the large solution cell. However, at 4 min already a significant proportion of Mo–Mo contributions can be detected (Fig. 6, Table 5), indicating a significant amount of Mo colloid formation. Although the accuracy of the higher Mo–Mo shells is low, the Mo particles detected should be of considerable size for these shells to be visible and significant in the Fourier transforms. Again, this irreversible deactivation of the Mo is observed at much shorter timescales compared to the reactions in the large solution cell (see Fig. 6). As said, the higher equivalents of AlMe_3 (1:20 as in the large solution cell, and 1:32) led to an almost immediate Mo precipitation, indicating the reaction rate for this Mo complex, of at least the deactivation part, is much faster in the stopped-flow than in the large solution cell.

Reactions of the tri-bromide analogues were, as also observed in the large solution cell, significantly slower than the tri-chloride complexes. The $[\text{MoBr}_3(\text{SBz})]$ complex was reacted with 20 equivalents of AlMe_3 , followed with time-resolved XAS, and the EXAFS after 4 min of reaction was analysed and presented in Table 6. As for the end-state analyses, only a small loss in bromide ligand was observed, whereas the SBz ligand remains intact and no significant Mo–C can be fitted reliably. The amount of Mo–Br contributions still present is slightly higher compared to the large solution

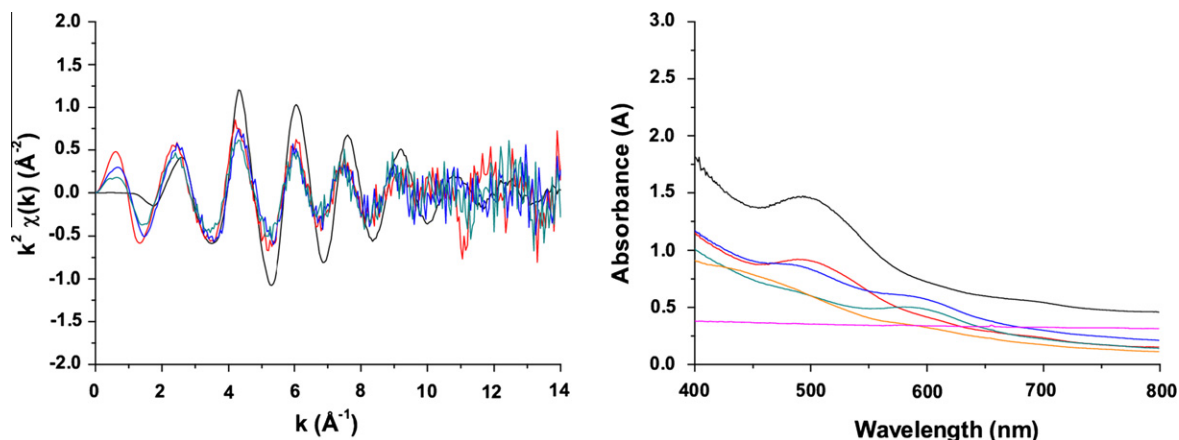


Fig. 7. Combined time-resolved UV-Vis and QEXAFS data on the reaction of **[MoCl₃(SNS)]** (25 mM in toluene) with 20 equivalents of AlMe₃ at $t = 0$ (black), $t = 1$ min (red), $t = 2.5$ min (blue), $t = 7$ min (green), $t = 18$ min (orange), $t = 19$ min (pink). (For interpretation of the references to colour in this figure legend, the reader is referred to the web version of this article.)

cell, which corresponds to the shorter reaction time in the stopped-flow. Here, no clear effect upon reaction rate is observed going from the large volume large solution cell to the small volume stopped-flow cuvette.

3.4. Freeze-quench study of the alkylation of **[MoBr₃(SBz)]**

The BioLogic stopped-flow quench system was modified and an air and moisture tight freeze-quench accessory developed to allow us to use the millisecond time resolution of the stopped-flow apparatus to select and isolate different intermediates, freeze-quench them and keep them frozen to allow long EXAFS experimentation to be conducted (if required). The reaction solutions are sprayed directly into a Kapton[®] tube immersed in liquid nitrogen. The required freezing time for the volume of 75 μ L is very difficult to assess and measure, but estimated to be less than 1 s in total. The entire system was thoroughly tested with a very air and moisture sensitive system [(TiCp₂)₂(μ -Cl)₂] (green) [38], to ensure its functionality. The deep green dimeric Ti solution (in toluene) system is very sensitive to O₂ and rapidly changes to yellow upon oxidation. Glove box tests showed that the solid oxidised at O₂ levels >5 ppm. After taking the solution through the stopped-flow and freezing it into the Kapton[®] tube, the solution remained green, indicating a O₂ free system was established.

To validate the freeze-quench approach, we have investigated the reaction of **[MoBr₃(SBz)]** with 20 equivalents of AlMe₃. Initially, the starting Mo solution is injected in the capillary, frozen and measured. Good quality transmission and fluorescence data could be obtained for these Mo systems, with identical EXAFS spectra. Analysis of the EXAFS revealed that the same structural parameters were obtained as for the solution state structure. The reaction was then freeze-quenched after 5 s and again after 5 min of reaction, to compare to the time-resolved data as obtained in the stopped-flow. Fig. 8 shows the EXAFS data obtained for the different frozen intermediates alongside the solution starting structure. The signal to noise of the frozen data is somewhat lower compared to the time-resolved data in the cuvette. This can be easily improved by acquiring more spectra and measuring longer (but this was not done here due to time constraints). In practice, it turns out (above) that this reaction is rather slow, so quick freezing did not necessarily reveal any new intermediates. It did however allow us to probe the reaction at identical conditions (20 equivalents AlMe₃) as the time-resolved XAS. We should then in principle be observing the same intermediates and thus prove the functionality of the stopped-flow freeze-quench. Moreover, the bromide ana-

logue allows us to distinguish between ligand and halide easier (compared to chlorine complex). As for the time-resolved data, a small decrease in the EXAFS, especially in the $5 < k < 11 \text{ \AA}^{-1}$ region, in time is observed. Comparing the Fourier transforms of the three data sets shows nicely the decrease in intensity on the high R side, i.e. where the Mo-Br contribution is. The analyses of both data sets, as presented in Table 6, show again the partial removal of Br, without dissociation of the SBz ligand, which closely corresponds to the time-resolved data. In addition, the freeze-quench set-up now gives access to good quality EXAFS data 5 s after mixing, something which could not be obtained using QEXAFS as performed (Mo K-edge QEXAFS time resolution possible at our beamtime periods were 20–30 s/spectrum, or 1–3 min/spectrum).

The combination of experiments as performed in this study clearly show the stepwise displacement of the halide ligand upon activating **[MoX₃(L)]** complexes with AlMe₃, forming mixed alkyl and halide mononuclear complexes, see Fig. 5, as was suggested for some Cr systems [13]. The high Mo K-edge energy allows time-resolved stopped-flow XAS experimentation down a time resolution of 20 s per spectrum (for good S/N quality data to allow EXAFS analyses). The new freeze-quench methodology is an extension to the stopped-flow with a freeze-quenching time of less than a second, thereby giving access to a time regime not accessible with the time-resolved XAS as performed.

Although the Mo complexes have shown a very low catalytic activity towards ethene oligomerisation [22], it is reasonable that the Mo systems undergo similar chemistry in the early stages of activation. This is in fact what we see. The stepwise displacement of the halide forming **[Mo(CH₃)₃(L)]** is in agreement with our previous studies on the AlMe₃ activation of comparable **[CrCl₃(L)]** complexes [14]. Whereas literature reports on halide-bridged dimer formation at low Cr:Al ratios [12], dimeric Mo species are not observed in this study at high Mo:Al ratios, i.e. ratios more relevant to industrial conditions [2]. Going from the Cr to the Mo analogues, a clear decrease in reaction rate was observed, as expected. However, also a significant dependence of reaction kinetics is observed upon halide ligand, with the **[MoCl₃(L)]** being much faster than the **[MoBr₃(L)]** analogues. It is difficult to immediately rationalise this difference, since the exact substitution mechanism is unknown and may in fact be different for the two types of complexes. The reaction can be based upon a dissociative or Lewis acid approach, with Al-Cl versus Al-Br bond formations being the rate determining steps. Moreover, at the high concentrations of reactants as used in this study, the activation reaction is in competition with the complex dissociation reaction as observed, especially for

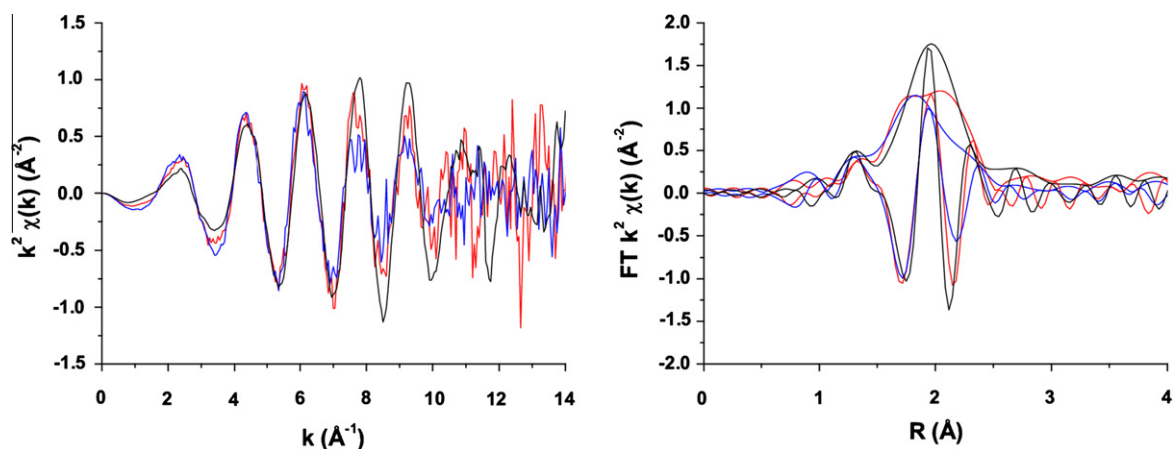


Fig. 8. Raw k^2 -weighted EXAFS data (a) and Fourier Transform ($1.8 < k < 12$) (b) data on the $[\text{MoBr}_2(\text{SBz})]$ solution (black), with 20 equivalents of AlMe_3 FQ after 5 s (red) and FQ after 5 min (blue) samples. (For interpretation of the references to colour in this figure legend, the reader is referred to the web version of this article.)

the chloride analogues. This is not necessarily a problem for the catalysis, since we are only looking at the first stage of activation here, and all subsequent catalysis reaction steps with ethene may make the formed complexes more stable. This study does provide insights in the low overall catalytic activity and deactivation of these complexes, as observed in catalytic tests.

4. Conclusions and outlook

We have used time-resolved Mo K-edge EXAFS in a stopped-flow system to probe the first stage of activation of the Mo analogues of the industrially important ethene trimerisation catalysts and compared the results with start and end-state studies. The results demonstrate that treatment of the Mo complex solution with excess AlMe_3 leads to halide loss, forming $[\text{Mo}(\text{CH}_3)_3(\text{L})]$, and provides strong evidence that dinuclear species with direct Mo–Mo bonds or halide-bridged dimers are not present under the conditions examined (1:20 Mo:Al). At the high AlMe_3 ratios used, with the complexes investigated, the activation reaction is in competition with the deactivation reaction, especially for the trichloride complexes, providing insights in the low overall catalytic activity and deactivation as has been reported for these systems under real catalytic conditions [21]. Whereas the use of the stopped-flow for time-resolved homogeneous catalysis has been reported before [17,18,20], we now have also developed a freeze-quench attachment which takes advantage of the excellent volume and timescale control offered by the stopped-flow instrument, and allows reaction mixtures to be frozen (to liquid nitrogen temperature) within 1 s of mixing under anaerobic conditions. This allows reactive, short-lived intermediate species to be trapped and enables EXAFS data collections to be conducted on these over long timescales (as required for 3d transition metals with low X-ray absorption edge energies and for low concentrations). The freeze-quench experiment can be performed in fluorescence mode, which is essential for studying systems with low energy absorption edges (e.g. Cr, Sc, etc.). A key advantage is that the much longer data acquisition times associated with these 3d metal systems are easily accommodated. This technique has great potential for probing reactive intermediates in many homogeneous catalytic systems, down to the seconds timescale with the freeze-quench procedure taking about 1 s. In fact, the methodology increases the XAS time resolution for these systems with a factor of 4,000–10,000 (1 s compared to 1–4 h as before). Not only reactions can be quenched and measured, also in case of samples which are easily affected by beam damage (which is not the case in this study), beam damage

can be prevented or at least decreased by keeping the samples at low temperature. Further experiments using this approach to examine the catalytic process associated with the $[\text{CrCl}_3(\text{SNS})]$ ethene trimerisation system are now planned.

Acknowledgments

The ESRF is gratefully acknowledged for provision of beamtime (26-01-829) and the staff with their help. The Swiss Light Source, PSI, Villigen, Switzerland is gratefully acknowledged for provision of beamtime, with EU funding under EU Project FP7 ELISA. The Diamond Light Source for beamtime provision under project SP7046-1. MT gratefully acknowledges the EPSRC (EP/E060404/1), SAB and PPW the EPSRC (EP/F032463/1). Dr. M. Webster is gratefully acknowledged for help with the X-ray crystallography.

Appendix A. Supplementary material

Supplementary data associated with this article can be found, in the online version, at [doi:10.1016/j.jcat.2011.10.015](https://doi.org/10.1016/j.jcat.2011.10.015).

References

- [1] J. Skipinska, Chem. Rev. 91 (1991) 613.
- [2] D.S. McGuinness, Chem. Rev. 111 (2011) 2321 (and references therein).
- [3] J.T. Dixon, M.J. Green, F.M. Hess, D.H. Morgan, J. Organometal. Chem. 689 (2004) 3641.
- [4] D.F. Wass, Dalton Trans. (2007) 816.
- [5] W. Janse van Rensburg, C. Grove, J.P. Steynberg, K.B. Stark, J.J. Huyser, P.J. Steynberg, Organometallics 23 (2004) 1207.
- [6] (a) D.S. McGuinness, P. Wasserscheid, W. Keim, J.T. Dixon, J.J.C. Grove, C. Hu, U. Englert, Chem. Commun. (2003) 334; (b) D.S. McGuinness, P. Wasserscheid, W. Keim, D.H. Morgan, J.T. Dixon, A. Bollmann, H. Maumela, F.M. Hess, U. Englert, J. Am. Chem. Soc. 125 (2003) 5272; (c) D.S. McGuinness, P. Wasserscheid, D.H. Morgan, J.T. Dixon, Organometallics 24 (2005) 552.
- [7] A. Carter, S.A. Cohen, N.A. Cooley, A. Murphy, J. Scutt, D.F. Wass, Chem. Commun. (2002) 858.
- [8] E.Y.-X. Chen, T.J. Marks, Chem. Rev. 100 (2000) 1391.
- [9] D.S. McGuinness, D.B. Brown, R.P. Tooze, F.M. Hess, J.T. Dixon, A.M.Z. Slawin, Organometallics 25 (2006) 3605.
- [10] D.S. McGuinness, A.J. Rucklidge, R.P. Tooze, A.M.Z. Slawin, Organometallics 26 (2007) 2561.
- [11] A.J. Rucklidge, D.S. McGuinness, R.P. Tooze, A.M.Z. Slawin, D.A. Pelletier, M.J. Hanton, P.B. Webb, Organometallics 26 (2007) 2782.
- [12] (a) C. Temple, A. Jabri, P. Crewdson, S. Gambarotta, I. Korobkov, R. Duchateau, Angew. Chem. Int. Ed. 45 (2006) 7050; (b) A. Jabri, C. Temple, P. Credson, S. Gambarotta, I. Korobkov, R. Duchateau, J. Am. Chem. Soc. 128 (2006) 9238.
- [13] S. Lui, R. Pattacini, P. Braunstein, Organometallics 30 (2011) 3549.

- [14] J.O. Moulin, J. Evans, D.S. McGuinness, G. Reid, A.J. Rucklidge, R.P. Tooze, M. Tromp, *Dalton Trans.* (2008) 1177.
- [15] N. Yoshida, T. Matsushita, S. Saigo, H. Oyanagi, H. Hashimoto, M. Fujimoto, J. Chem. Soc. Chem. Commun. (1990) 354.
- [16] M.B.B. Abdul Rahman, P.R. Bolton, J. Evans, A.J. Dent, I. Harvey, S. Diaz-Moreno, *Faraday Discuss.* 122 (2002) 211.
- [17] M. Tromp, J.R.A. Sietsma, J.A. van Bokhoven, G.P.F. van Strijdonck, R.J. van Haaren, A.M.J. van der Eerden, P.W.N.M. van Leeuwen, D.C. Koningsberger, *Chem. Commun.* (2003) 128.
- [18] M. Tromp, S.S. van Berkel, A. van den Hoogenband, M.C. Feiters, B. de Bruin, S.G. Fiddy, J.A. van Bokhoven, P.W.N.M. van Leeuwen, G.P.F. van Strijdonck, D.C. Koningsberger, *Organometallics* 29 (2010) 3085.
- [19] J. Evans, A. Puig-Molina, M. Tromp, *MRS Bull.* 32 (2007) 1038.
- [20] G. Smolentsev, G. Guilera, M. Tromp, S. Pascarelli, A.V. Soldatov, *J. Chem. Phys.* 130 (2009) 174508.
- [21] S.P. Downing, M.J. Hanton, A.M.Z. Slawin, R.P. Tooze, *Organometallics* 28 (2009) 2417.
- [22] O. Kleifeld, A. Frenkel, J.M. Martin, I. Sagi, *Nat. Struct. Biol.* 10 (2003) 98.
- [23] F. Stoffelbach, D. Saurens, R. Poli, *Eur. J. Inorg. Chem.* (2001) 2699.
- [24] B.E. Owens, R. Poli, A.L. Rheingold, *Inorg. Chem.* 28 (1989) 1456.
- [25] D.S. McGuinness, P. Wasserscheid, W. Kiem, D.H. Morgan, J.T. Dixon, A. Bollmann, H. Maumela, F.M. Hess, U. Englert, *J. Am. Chem. Soc.* 125 (2003) 5272.S3.
- [26] E. Jordon, *Anal. Chem.* 40 (1968) 2150.
- [27] D. Sellmann, L. Zapf, *J. Organomet. Chem.* 289 (1985) 57.
- [28] (a) G.M. Sheldrick, SHELXS-97, Program for Crystal Structure Solution, University of Göttingen, Germany, 1997;
- (b) G.M. Sheldrick, SHELXL-97, Program for Crystal Structure Refinement, University of Göttingen, Germany, 1997;
- (c) Flack, *Acta Crystallogr. Sect. A* 39 (1983) 876.
- [29] M. Tromp, 'Developments of Time-Resolved XAFS Techniques: Applications in Homogeneous Catalysis', Ph.D. Thesis, Utrecht, The Netherlands, 2004, pp. 20–23.
- [30] S. Nikitenko, A.M. Beale, A.M.J. van der Eerden, S.D.M. Jacques, O. Leynaud, M.G. O'Brien, D. Detollenaere, R. Kaptein, B.M. Weckhuysen, W. Bras, *J. Synchrotron Radiat.* 15 (2008) 632–640.
- [31] A.J. Dent, G. Cibir, S. Ramos, A.D. Smith, S.M. Scott, L. Varandas, M.R. Pearson, N.A. Krumpa, C.P. Jones, P.E. Robbins, *J. Phys.: Conf. Ser.* 190 (2009) 01203.
- [32] M.J. Newville, *J. Synchrotron Radiat.* 8 (2001) 322.
- [33] B. Ravel, M.J. Newville, *J. Synchrotron Radiat.* 12 (2005) 537.
- [34] (a) C.D. Beard, L. Carr, M.F. Davis, J. Evans, W. Levason, L.D. Norman, G. Reid, M. Webster, *Eur. J. Inorg. Chem.* (2006) 4399;
- (b) G.J. Grant, K.E. Rogers, W.N. Setzer, D.G. VanDerveer, *Inorg. Chim. Acta* 234 (1995) 35;
- (c) R.E. Wolf, J.R. Hartman, J.M.E. Storey, B.M. Foxman, S.R. Cooper, *J. Am. Chem. Soc.* 109 (1987) 4328.
- [35] F.A. Cotton, Multiple bonds between metal atoms, in: F.A. Cotton, C.A. Murillo, R.A. Walton (Eds.), third ed., Springer, 2005. ISBN 978-0-387-25084-7.
- [36] J.O. Moulin, 'X-Ray Absorption Spectroscopy for the Study of a Homogeneous Catalysis System based Upon Chromium', Ph.D. Thesis, Southampton, United Kingdom, 2006.
- [37] A.B.P. Lever, *Inorganic Electronic Spectroscopy*, second ed., Elsevier, Canada, 1984 (chapter 5).
- [38] S.J. Nietner Burgmayer, *J. Chem. Ed.* 75 (1998) 460.